

## Article

# Effect of Buoyancy Force on an Unsteady Thin Film Flow of $\text{Al}_2\text{O}_3$ /Water Nanofluid over an Inclined Stretching Sheet

Sumayyah Alabdulhadi <sup>1,2</sup>, Sakhinah Abu Bakar <sup>1</sup>, Anuar Ishak <sup>1,\*</sup> , Iskandar Waini <sup>3</sup> and Sameh E. Ahmed <sup>4,5</sup> 

<sup>1</sup> Department of Mathematical Sciences, Faculty of Science and Technology, Universiti Kebangsaan Malaysia (UKM), Bangi 43600, Selangor, Malaysia

<sup>2</sup> Department of Mathematics, Faculty of Science, Qassim University, Buraydah 52571, Saudi Arabia

<sup>3</sup> Fakulti Teknologi Kejuruteraan Mekanikal dan Pembuatan, Universiti Teknikal Malaysia Melaka, Hang Tuah Jaya, Durian Tunggal 76100, Melaka, Malaysia

<sup>4</sup> Department of Mathematics, Faculty of Science, King Khalid University, Abha 62529, Saudi Arabia

<sup>5</sup> Department of Mathematics, Faculty of Science, South Valley University, Qena 83523, Egypt

\* Correspondence: anuar\_mi@ukm.edu.my

**Abstract:** The present study looks at the heat transfer and the unsteady thin film flow of  $\text{Al}_2\text{O}_3$  water nanofluid past an inclined stretching sheet having a buoyancy force effect. The boundary value problem solver (bvp4c) package in Matlab is utilized in solving the converted set of ordinary differential equations (ODEs). The multi-shape  $\text{Al}_2\text{O}_3$  nanoparticles' impact with respect to the flow as well as heat transfer characteristics are studied and visually displayed for certain governing parameter values, which include the mixed convection, inclination angle, magnetic, slip, and Biot number. Thus, the skin friction coefficient and the local Nusselt number are also determined. Here, the platelet shape of  $\text{Al}_2\text{O}_3$  nanoparticles possesses a high heat transfer and flow rate based on the outcomes. In addition, increasing the slip and magnetic parameters improves the temperature, whereas increasing the buoyancy and inclination angle parameters has reverse effects. The results also show that increasing the unsteadiness parameter and the magnetic parameter reduces the film thickness.

**Keywords:** thin film; nanofluid; inclined sheet; shape factor; unsteady flow; convective boundary conditions

**MSC:** 76D10



**Citation:** Alabdulhadi, S.; Abu Bakar, S.; Ishak, A.; Waini, I.; Ahmed, S.E. Effect of Buoyancy Force on an Unsteady Thin Film Flow of  $\text{Al}_2\text{O}_3$ /Water Nanofluid over an Inclined Stretching Sheet.

*Mathematics* **2023**, *11*, 739. <https://doi.org/10.3390/math11030739>

Academic Editors: Roman Parovik, Kholmat Mahkambaevich Shadimetov and Abdullo Rakhmonovich Hayotov

Received: 24 December 2022

Revised: 17 January 2023

Accepted: 28 January 2023

Published: 1 February 2023



**Copyright:** © 2023 by the authors. Licensee MDPI, Basel, Switzerland. This article is an open access article distributed under the terms and conditions of the Creative Commons Attribution (CC BY) license (<https://creativecommons.org/licenses/by/4.0/>).

## 1. Introduction

Over the last few decades, the topic of improving heat transfer in industrial applications has been of great relevance. The majority of applications use pure fluids, such as water, oil, and ethylene, as cooling liquids. However, these fluids have low heat transfer rates. To improve heat transfer rates, nanometer-sized particles are scattered into the base fluid to improve its thermal performance and rate of heat transfer [1]. Choi and Eastman were the first to refer to this combination as nanofluid [2]. The addition of nanoparticles into the base fluid significantly improves the heat transfer and thermal conductivity of these fluids. Since this research, nanofluids have been extensively employed in heating and cooling systems, nuclear applications, power generation, medicine, electronics, automobiles, and other applications [3–6]. Consequently, numerous numerical and experimental studies have been performed to investigate the nanofluids' properties and behaviors in various aspects [7–13]. Sajjadi et al. [14] scrutinized the MHD natural convection flow of a nanofluid in a 3-D cavity where the sinusoidal temperature is distributed on a side wall. They concluded that the augmentation of the volumetric fraction of nanoparticles accelerates the rate of heat transfer. Afterwards, Atashafrooz et al. [15] studied the entropy generation due to an

inclined step using two types of nanofluids. According to the predictions, they found that the  $\text{Al}_2\text{O}_3$ /water nanofluid is better suited for the hydrothermal system's ideal design.

The boundary layer flow originated from a stretching sheet is of great significance as a result of its critical role in industry and engineering. Crane [16] was the pioneer in investigating the 2D boundary layer flow brought on by a stretching sheet. Furthermore, Gupta and Gupta [17] extended earlier research by considering the case of stretching surfaces under the effect of suction or blowing. Since then, several authors have been working to solve the boundary layer flow issue with respect to a stretching surface by considering various nanofluids under varied physical conditions, such as Sharma et al. [18], Zokri et al. [19], Kho et al. [20], Daniel et al. [21], Ahmed et al. [22], Kho et al. [23], and Ibrahim and Negera [24]. Numerical solutions of MHD Maxwell nanofluid flow induced by stretching surface was scrutinized by Prasannakumara [25]. He reported that the surface drag force is enhanced by increasing the volume fraction. Hazarika et al. [26] used a numerical method to resolve the stretching sheet problem for three different types of nanoparticles, including Ferrous Ferric Oxide ( $\text{Fe}_3\text{O}_4$ ), Silver (Ag), and Copper (Cu). They claimed that  $\text{Fe}_3\text{O}_4$ -water nanofluid always overshoots the velocity, followed by Cu and Ag-water nanofluid, although the temperature profiles exhibit the opposite behaviours.

Furthermore, the horizontal and vertical positions of the flat plate have been utilized in numerous research studies. The inclined flat plate, on the other hand, has received less attention. Thus, it is beneficial to examine the fluid flow induced by an inclined flat plate at diverse angles as are used in many engineering processes. In addition, Gupta et al. [27] examined the radiation and chemical reactions on the laminar magnetohydrodynamics (MHD) stagnation point flow, including heat transfer in a non-Newtonian nanofluid caused by an inclined stretching surface. Usman et al. [28] investigated the combination effects of thermal and velocity slips on Casson nanofluid flow past a permeable inclined stretching cylinder. They discovered that the thermophoresis and Brownian motion impacts play a prominent role in the concentration and thermal boundary layers. Moreover, the unsteady MHD flow using Eyring-Powell nanofluid due to an inclined permeable stretching surface was numerically examined by Kumar and Srinivas [29]. They considered the influences of Joule heating and thermal radiation. Afterwards, a numerical computation of MHD hybrid nanofluid flow driven by an inclined sheet was scrutinized by Soomro et al. [30] who found that  $\text{Al}_2\text{O}_3$ -Cu/water hybrid nanofluid increased the heat transfer rate in contrast to the basic Cu/water nanofluid.

Many scholars have recently become interested in problems with unsteady boundary layers because of their significant role in a variety of engineering issues. Start-up processes, for instance, denote the motions at rest in transit between one steady flow and another, as well as periodic working fluid motion [31]. Because of the extra time-based factors that impeded the separation of boundary layer and fluid motion pattern, unsteady boundary layer flow activity seems to behave differently than a steady flow [32,33]. The unsteady mixed convection flow, as well as heat transfer caused by a stretching vertical sheet, were examined by Ishak et al. [34]. Moreover, Ishak et al. [35] then looked at how MHD affected the unsteady flow, as well as heat transfer past a stretching surface, and deduced that the rate of heat transfer rises with a rise of the unsteadiness parameter. In contrast, an increment in the magnetic parameter results in a decrease in the heat transfer rate. Daniel et al. [36] performed an investigation on the unsteady MHD natural convection flow problem with respect to a viscous nanofluid due to a permeable shrinking surface which took into account the influences of chemical reaction, electric field, thermal radiation, and viscous dissipation. Dzulkipli et al. [37] also looked at the effect of slip on the unsteady stagnation-point flow and heat transfer caused by a porous exponentially shrinking/stretching surface. They claimed that there are dual solutions and noted that discovering the dual solutions in the case of suction is much simpler than in the case of injection. In addition, Waini et al. [1] examined the 2D unsteady heat transfer and hybrid nanofluid flow numerically concerning a shrinking/stretching surface. Dual solutions were found for a given range of the unsteadiness parameter. Thereafter, Waini et al. [38] employed a hybrid  $\text{Al}_2\text{O}_3$ -Cu/water

nanofluid produced by a permeable rigid sheet to conduct a temporal stability analysis of an unsteady stagnation point flow. A numerical analysis of the unsteady hybrid nanofluid flow brought on by a permeable stretching/shrinking cylinder was also carried out by Zainal et al. [39]. They stated that including the unsteadiness parameter significantly aided in the heat transfer deterioration.

Given the vital uses in industry and engineering—for instance, paper manufacture, polymer and foodstuff processing, wire thinning, crystal growth, and so on—the thin film flow has recently been a demanding research issue. A thin layer of liquid flows past a solid surface because of an external force acting on it, such as gravity, shear stress, or other factors known as film flow. For example, Wang [40] was the first to investigate the thin film flow problem due to an unsteady stretching surface. Later, Andersson et al. [41] improved the previous work by considering the analysis of heat transfer. In addition, Khan et al. [42] provided an analytical solution to the heat transfer problem and the second-grade fluid's thin film flow across a stretched surface in a porous medium. The effect of film thickness was explored, and it was discovered that, when film thickness decreases, the skin friction coefficient increases. In addition, Naganthran [43] reported the impacts of injection and thermocapillarity on the Carreau thin film flow, including heat transfer in relation to an unsteady stretching surface. It has been demonstrated that increasing the injection intensity and unsteadiness parameter reduces the film thickness, resulting in a rise in the convective heat transfer rate and skin friction coefficient. Afterwards, Naganthran [44] performed an investigation on the flow of the Carreau thin hybrid nanofluid film caused by an accelerating surface together with the melting heat transfer influence. They concluded that melting heat transfer slows the pace of heat transfer rate while having no effect on the liquid film thickness. Moreover, Ali et al. [45] utilized  $\text{Al}_2\text{O}_3$  nanofluid past a stretching sheet with convective boundary conditions in examining the unsteady thin film flow dynamic and heat transfer.

A fair amount of substantial analysis on the thin film flow due to a stretching sheet has been carried out by researchers. However, the thin film flow on an inclined stretching plate is rarely examined, motivating the current research to investigate the thin film flow on an inclined stretching surface. Under the multi-shape nanoparticles' effect, the primary goal of this research is to investigate the unsteady thin film flow as well as heat transfer with respect to the inclined stretching sheet in  $\text{Al}_2\text{O}_3$ /water nanofluid. Moreover, the convective boundary conditions and buoyancy force effects have also been considered. By employing the similarity transformation, the provided system is transformed to a system of ordinary differential equations (ODEs) which are later numerically solved using the boundary value problem solver (bvp4c) available in Matlab software. This research has investigated the impacts of the distinct factors with regard to the temperature fields as well as the velocity fields. In addition, the acquired numerical findings and the published results available in the literature have been compared for the purpose of validation. The above literature review reveals that no studies of this kind have been performed by any other researchers.

## 2. Mathematical Formulation

Consider a thin film flow and heat transfer in a nanofluid across an unsteady stretching sheet. Here, the matching physical model is portrayed in Figure 1, with the  $x$ -axis parallel to the plate and the  $y$ -axis perpendicular to it. Also, the current study examines the effects of four different nanoparticle shapes, including the platelet, cylinder, brick, and sphere-shaped nanoparticles. It is assumed that the base fluid and the multi-shape nanoparticles are in thermal equilibrium. Further,  $U_w = \frac{bx}{1-at}$  represents the stretching surface velocity in the  $x$  direction, where  $t$  is time and  $a, b$  are dimensional constants. The uniform magnetic field is assumed as  $B(t) = \frac{B_0}{\sqrt{1-at}}$ , and the temperature distribution at the wall is represented by  $T_w = T_\infty + T_0\left(\frac{x}{(1-at)^2}\right)$ , where  $T_\infty$  and  $T_0$  are ambient temperature and constant reference temperature, see Ref. [45].

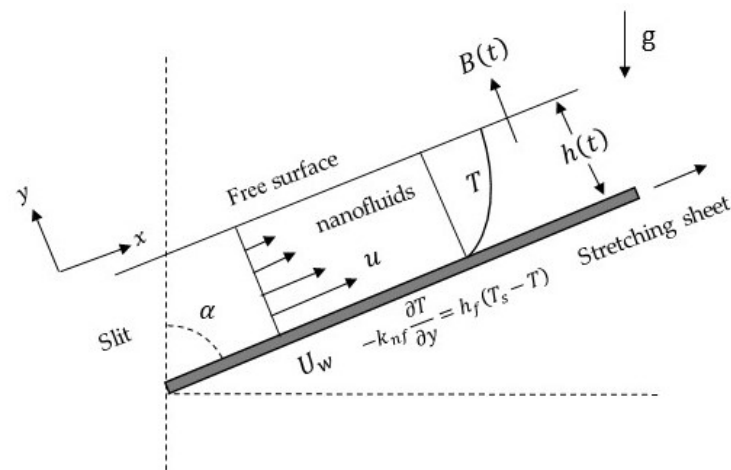


Figure 1. Schematic diagram of the present study.

From all of the considerations above and using the nanofluid model introduced by Tiwari and Das [46], the boundary layer governing equations for the present problem are given by [45,47].

$$\frac{\partial u}{\partial x} + \frac{\partial v}{\partial y} = 0, \tag{1}$$

$$\frac{\partial u}{\partial t} + u \frac{\partial u}{\partial x} + v \frac{\partial u}{\partial y} = \frac{\mu_{nf}}{\rho_{nf}} \frac{\partial^2 u}{\partial y^2} - \frac{\sigma_{nf}}{\rho_{nf}} B(t)^2 u + \frac{(\rho\beta^*)_{nf}}{\rho_{nf}} g(T - T_\infty) \cos \alpha, \tag{2}$$

$$\frac{\partial T}{\partial t} + u \frac{\partial T}{\partial x} + v \frac{\partial T}{\partial y} = \frac{k_{nf}}{(\rho c_p)_{nf}} \frac{\partial^2 T}{\partial y^2}, \tag{3}$$

subject to the boundary conditions [45].

$$\begin{aligned} y = 0 : u &= U_w + Av_f \frac{\partial u}{\partial y}, v = 0, -k \frac{\partial T}{\partial y} = h_f [T_0 - T], \\ y = h(t) : \frac{\partial u}{\partial y} &= 0, \frac{\partial T}{\partial y} = 0, v = \frac{dh}{dt}. \end{aligned} \tag{4}$$

Here, the nanofluid velocity components along  $x$  and  $y$  directions are represented by  $u$  and  $v$ , respectively. Moreover,  $T$  is the fluid temperature,  $g$  is the gravitational acceleration,  $\alpha$  is the inclination angle,  $h(t)$  is the thickness of the film,  $A = A_0 \sqrt{1 - at}$  represent the velocity slip factor with constant  $A_0$ , and  $h_f = \frac{h_0}{\sqrt{1 - at}}$  denotes the convective heat transfer with  $h_0$  being constant. Furthermore,  $\rho_{nf}$ ,  $\mu_{nf}$ ,  $\sigma_{nf}$ ,  $(\rho\beta^*)_{nf}$ ,  $k_{nf}$ , and  $(\rho c_p)_{nf}$  denote the density, dynamic viscosity, electrical conductivity, diffusivity, thermal expansion coefficient, thermal conductivity, and the heat capacity of the nanofluid, respectively, which are defined as the following [45,48]:

$$\begin{aligned} \rho_{nf} &= (1 - \varphi)\rho_f + \varphi\rho_s, (\rho c_p)_{nf} = (1 - \varphi)(\rho c_p)_f + \varphi(\rho c_p)_s, \\ \mu_{nf} &= \mu_f(1 + A_1\varphi + A_2\varphi^2), \sigma_{nf} = \sigma_f(1 - \varphi) + \varphi\sigma_s, \\ (\rho\beta^*)_{nf} &= (1 - \varphi)(\rho\beta^*)_f + \varphi(\rho\beta^*)_s, \\ \frac{k_{nf}}{k_f} &= \frac{k_s + (m-1)k_f + (m-1)(k_s - k_f)\varphi}{k_s(m-1)k_f - (k_s - k_f)\varphi}, \end{aligned} \tag{5}$$



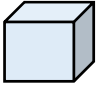

where  $\varphi$  is the volume fraction of the nanoparticle, and the viscosity enhancement heat capacitance coefficients are symbolized by  $A_1$  and  $A_2$ . Meanwhile, the base fluid, nanofluid and nanoparticles are signified as the subscripts  $f$ ,  $nf$  and  $s$ , respectively, while  $m$  implies the shape factor. Furthermore, it is important to note that the convective heat transfer property of nanofluids depends on the thermophysical characteristics of the suspended particles and the base fluid; the flow structure and pattern; the dimensions and shape of

nanoparticles; and the volumetric fraction of nanoparticles. The thermophysical properties, shape factor of various geometry in this study, and coefficients of viscosity for Al<sub>2</sub>O<sub>3</sub> nanoparticles along with water are presented in Tables 1 and 2 [49–51].

**Table 1.** Thermophysical properties of Al<sub>2</sub>O<sub>3</sub> and water.

Physical Properties	Al <sub>2</sub> O <sub>3</sub>	H <sub>2</sub> O
$\rho(\text{kgm}^{-3})$	3970	997.1
$k(\text{W m}^{-1}\text{K}^{-1})$	40	0.613
$c_p(\text{J kg}^{-1}\text{K}^{-1})$	765	4179
$\sigma(\text{s m}^{-1})$	16.5	5.50
$\beta^* \times 10^{-5}(\text{K}^{-1})$	0.85	21

**Table 2.** Viscosity and shape factor values of nanoparticles.

Nanoparticle Shapes	Platelets	Cylinder	Brick	Sphere
				
Parameters				
$A_1$	37.1	13.5	1.9	2.5
$A_2$	612.6	904.4	471.4	6.5
Shape factors (m)	5.72	4.82	3.72	3.0

Next, the following similarity transformations are employed [45]:

$$\theta(\eta) = \frac{T - T_\infty}{T_w - T_\infty}, \eta = \sqrt{\frac{b}{\nu_f(1-at)}}y, \psi = \sqrt{\frac{b\nu_f}{1-at}}xf(\eta), \tag{6}$$

where  $\psi$  indicates the stream function which is defined as  $u = \frac{\partial\psi}{\partial y}$ , and  $v = -\frac{\partial\psi}{\partial x}$ ,  $\nu_f$  denotes the kinematic viscosity and  $\beta$  is the dimensionless film thickness, expressed as

$$\beta = \sqrt{\frac{b}{\nu_f(1-at)}}h(t) \tag{7}$$

which will eventually result in

$$\frac{dh}{dt} = -\frac{a\beta}{2} \sqrt{\frac{\nu_f}{b(1-at)}}, \tag{8}$$

implying that in the similarity variables (6) in Equations (1)–(4), Equation (1) is identically fulfilled while the remaining equations become

$$\varepsilon_1 f'''(\eta) - M\varepsilon_3 f'(\eta) - S\left[f'(\eta) + \frac{\eta}{2}f''(\eta)\right] - f'^2(\eta) + f(\eta)f''(\eta) + \varepsilon_4\lambda\theta\cos\alpha = 0, \tag{9}$$

$$\frac{\varepsilon_2}{Pr}\theta''(\eta) - \frac{S}{2}(4\theta(\eta) + \eta\theta'(\eta)) - \theta(\eta)f'(\eta) + \theta'(\eta)f(\eta) = 0, \tag{10}$$

with the transformed boundary conditions:

$$\begin{aligned} \eta = 0 : f(0) = 0, f'(0) = 1 + Kf''(0), \theta'(0) = -\frac{k_f}{k_{nf}}Bi(1 - \theta(0)), \\ \eta = \beta : f(\beta) = \frac{S\beta}{2}, f''(\beta) = 0, \theta'(\beta) = 0. \end{aligned} \tag{11}$$

Here,  $M$  is the magnetic parameter,  $S$  is the unsteadiness parameter,  $Pr$  is the Prandtl number,  $K$  is the slip parameter,  $Bi$  is the Biot number, and  $\lambda$  is the buoyancy or mixed convection parameter, which are defined as

$$M = \frac{\sigma_f B_0^2}{\rho_{nf} b}, S = \frac{a}{b}, Pr = \frac{(\rho c_p)_f v_f}{k_f}, K = A \sqrt{\frac{v_f U_w}{x}} = A_0 \sqrt{v_f b},$$

$$Bi = \frac{h_f}{k_f} \sqrt{\frac{x v_f}{U_w}} = \frac{h_0}{k_f} \sqrt{\frac{v_f}{b}}, \lambda = \frac{Gr}{Re_x^2} = \frac{T_0 g \beta_f^*}{b^2},$$
(12)

where  $Gr = \frac{g \beta_f^* (T_w - T_\infty) x^3}{v_f^2}$  and  $Re_x = \frac{U_w x}{v_f}$  represent, respectively, the Grashof number and the local Reynold number [52]. Notice that  $\lambda > 0$  and  $\lambda < 0$  respectively refer to the assisting and opposing flows. Further,  $\epsilon_1, \epsilon_2, \epsilon_3,$  and  $\epsilon_4$  are constants and are given by

$$\epsilon_1 = \frac{1 + A_1 \varphi + A_2 \varphi^2}{1 - \varphi + \varphi \left( \frac{\rho_s}{\rho_f} \right)}, \epsilon_2 = \frac{\frac{k_{nf}}{k_f}}{1 - \varphi + \varphi \left( \frac{\rho c_p}_s}{\rho c_p}_f \right)}, \epsilon_3 = \frac{1 - \varphi + \varphi \left( \frac{\sigma_s}{\sigma_f} \right)}{1 - \varphi + \varphi \left( \frac{\rho_s}{\rho_f} \right)}, \epsilon_4 = \frac{(1 - \varphi)(\rho \beta^*)_f + \varphi(\rho \beta^*)_s}{((1 - \varphi)\rho_f + \varphi \rho_s) \beta_f^*}.$$
(13)

The skin friction coefficient and the Nusselt number are the physical quantities of interest which can be respectively expressed as

$$C_f = \frac{\tau_w}{\rho_f U_w^2}, Nu = \frac{q_w x}{k_f (T_w - T_\infty)},$$
(14)

where

$$\tau_w = \mu_{nf} \left( \frac{\partial u}{\partial y} \right)_{y=0}, q_w = -k_{nf} \left( \frac{\partial T}{\partial y} \right)_{y=0}.$$
(15)

By using (5) and inserting (15) into (14), the following relations are obtained:

$$C_f Re^{1/2} = (1 + A_1 \varphi + A_2 \varphi^2) f''(0), \quad Nu Re^{-1/2} = -\frac{k_{nf}}{k_f} \theta'(0).$$
(16)

### 3. Numerical Method

The package `bvp4c` in Matlab is utilized for solving the Equations (9) and (10) with the boundary conditions (11), numerically. The `bvp4c` solver, discussed by Shampine et al. [53], is based on the finite-difference method which uses the 3-stage Lobatto IIIa formula. Lobatto IIIa is a Runge-Kutta method that uses collocation and implicit trapezoidal rules. As a result, the collocation method is indicated by the `bvp4c` solver, which produces a C1-continuous solution with fourth-order accuracy uniformly in the interval in which the function is integrated. To begin using the `bvp4c` method, Equations (9) and (10) must be reduced to a set of first-order ordinary differential equations (ODEs), along with their boundary conditions (11), as follows:

$$f = y(1), f' = y(2), f'' = y(3), \theta = y(4), \theta' = y(5),$$

$$f''' = \frac{1}{\epsilon_1} (\mu \epsilon_3 y(2) + S [y(2) + \frac{\eta}{2} y(3)] + y(2)y(2) - y(1)y(3) - \epsilon_4 \lambda y(4) \cos \alpha),$$
(17)

$$\theta'' = \frac{Pr}{\epsilon_2} \left( \frac{S}{2} (3y(4) + \eta y(5)) + 2y(2)y(4) - y(1)y(5) \right).$$
(18)

The boundary conditions (11) become

$$ya(1), ya(2) - 1 - Kya(3), ya(5) + \frac{k}{k_{nf}} Bi(1 - ya(4)), yb(1) - \frac{s\beta}{2}, yb(3), yb(5).$$
(19)

Equations (17) and (18) form a set of five first-order ODEs together with six boundary conditions (19). Here, the crucial parameters are highlighted:  $S$  the unsteadiness parameter and  $\beta$  the film thickness parameter. There is a relationship between  $\beta$  and  $S$  that can lead to

the reduction of the six boundary conditions to five. To find the relationship of  $\beta$  and  $S$ , Equations (17) and (19) are solved first, and the initial guess value for  $\beta$  is provided by the `bvp4c` function in Matlab. The value of  $\beta$  is adjusted so that the condition  $f(\beta) = \frac{S\beta}{2}$  holds. It is achieved using trial-and-error processes. Equations (17)–(19) are solved utilizing the `bvp4c` solver for known values of  $S$  and  $\beta$ .

#### 4. Findings and Discussion

The boundary value problem solver (`bvp4c`) in Matlab software was applied in solving the mathematical model given in Equations (9)–(11) numerically for the chosen values of the inclination angle parameter  $\alpha$ , magnetic parameter  $M$ , slip parameter  $K$ , mixed convection parameter  $\lambda$ , and Biot number  $Bi$ . It is essential to note that the range with respect to multi-shape nanoparticles in a thin film past a stretching surface of  $Al_2O_3$ /water nanofluid affects both temperature profiles and velocity. The parameters' impact is depicted in tables and graphs. A comparative study of the results obtained by Abel et al. [54] and Ali et al. [45] are given in Table 3. The outcome shows a favorable agreement and ensures that the `bvp4c` scheme is highly accurate and effective. Moreover, the skin friction coefficient  $Re^{1/2}C_f$  for multi-shape nanoparticles is depicted in Table 4. The table demonstrates that, as the mixed convection parameter  $\lambda$  and slip parameter  $K$  increase, the skin friction  $Re^{1/2}C_f$  decreases. However, when the volume fraction parameter  $\varphi$  and magnetic parameter  $M$  increase, the skin friction  $Re^{1/2}C_f$  increases. In addition, the heat transfer rate  $Re^{-1/2}Nu$  is determined and presented in Table 5. Furthermore, it may also be noted that  $Re^{-1/2}Nu$  rises with the rising values of the inclination angle, Biot number, and mixed convection parameters. Meanwhile, the rising values of the slip and magnetic parameters tend to reduce the values of Nusselt number  $Re^{-1/2}Nu$ .

**Table 3.** Comparison of numerical results when  $M = K = \varphi = 0$ .

$S$	Abel et al. [54]		Ali et al. [45]		Present Result	
	$\beta$	$f''(0)$	$\beta$	$f''(0)$	$\beta$	$f''(0)$
0.4	4.981455	−1.134098	4.981468	−1.1340957	4.981466	−1.1340953
0.6	3.131710	−1.195128	3.131711	−1.1951252	3.131662	−1.1951202
0.8	2.151990	−1.245805	2.152021	−1.2458064	2.152011	−1.2458089
1.0	1.543617	−1.277769	1.543615	−1.2777693	1.543456	−1.2777079
1.2	1.1227780	−1.279171	1.127779	−1.2791718	1.127490	−1.2789750
1.4	0.8221033	−1.233545	0.8210317	−1.2335453	0.821016	−1.2335280
1.6	0.576176	−1.114941	0.5761743	−1.1149368	0.576061	−1.1147574
1.8	0.356390	−0.867416	0.3563871	−0.86741049	0.356236	−0.8670686

**Table 4.** Numerical values of skin-friction coefficient of multi-shape nanoparticles.

$K$	Physical Parameters			Platelets	Cylinder	Brick	Sphere
	$\varphi$	$M$	$\lambda$				
0.3	0.02	1.0	−2.0	1.681268266	1.489536298	1.247831761	1.133526940
0.5	—	—	—	1.433346676	1.258667526	1.039679801	0.937343360
0.7	—	—	—	1.253631522	1.093801740	0.893877800	0.802628774
0.5	0.02	1.0	−2.0	1.433346676	1.258667526	1.039679801	0.937343360
—	0.04	—	—	2.089089107	1.898450286	1.378306537	0.986750837
—	0.06	—	—	2.818098130	2.694112995	1.851288272	1.039162880
0.5	0.02	0.0	−2.0	1.163871057	1.028890432	0.859696435	0.778968598
—	—	0.5	—	1.318507553	1.161161807	0.961312098	0.869720683
—	—	1.0	—	1.433346676	1.258667526	1.039679801	0.937343360
0.5	0.02	1.0	−2.0	1.433346676	1.258667526	1.039679801	0.937343360
—	—	—	0.0	1.336031466	1.165473257	0.952085341	0.853015117
—	—	—	2.0	1.243847795	1.078097824	0.871460777	0.776276122

**Table 5.** Numerical values of Nusselt number for multi-shape nanoparticles.

Physical Parameters					Platelets	Cylinder	Brick	Sphere
<i>Bi</i>	$\alpha$	<i>K</i>	<i>M</i>	$\lambda$	$Re^{-1/2}Nu$			
2.0	$\pi/4$	0.5	1.0	−2.0	1.471184404	1.433486292	1.384283501	1.353043680
2.5	—	—	—	—	1.670669380	1.628171211	1.572161775	1.536832098
3.0	—	—	—	—	1.836441722	1.789956021	1.728163960	1.689397686
3.0	$\pi/6$	0.5	1.0	−2.0	1.833310838	1.786265359	1.723415633	1.683998156
—	$\pi/4$	—	—	—	1.836441722	1.789956021	1.728163960	1.689397686
—	$\pi/3$	—	—	—	1.840419312	1.794618692	1.734099222	1.696099546
3.0	$\pi/4$	0.3	1.0	−2.0	1.878381703	1.833316358	1.773533127	1.735593784
—	—	0.5	—	—	1.836441722	1.789956021	1.728163960	1.689397686
—	—	0.7	—	—	1.802096137	1.754817989	1.692274249	1.652735779
3.0	$\pi/4$	0.5	0.0	−2.0	1.875238410	1.830120581	1.770130660	1.732319575
—	—	—	0.5	—	1.853305927	1.807347347	1.746879653	1.708144155
—	—	—	1.0	—	1.836441722	1.789956021	1.728163960	1.689397686
3.0	$\pi/4$	0.5	1.0	−2.0	1.836441722	1.789956021	1.728163960	1.689397686
—	—	—	—	0.0	1.849584549	1.805260139	1.747406942	1.710956457
—	—	—	—	2.0	1.861624634	1.819046955	1.764227314	1.729451205

Figure 2 illustrates the effect of multi-shape nanoparticles with respect to the film thickness  $\beta$  of  $Al_2O_3$  nanofluids. In this case, the remaining physical parameters remain constant. Provided that the nanoparticles' shape changes, the film thickness also drastically changes. Furthermore, the velocity profile  $f'(\eta)$  and film thickness  $\beta$  accelerate for the platelet-shaped nanoparticles and decelerate for the brick, cylinder, and sphere-shaped nanoparticles. Figure 3 shows the impact of the slip parameter  $K$  on the temperature profile  $\theta(\eta)$  for multi-shape nanoparticles. The temperature profile  $\theta(\eta)$  for each multi-shape nanoparticle increases as the slip parameter  $K$  rises. The enhancement of the slip parameter has resulted in acceleration of the fluid within the boundary layer. Additionally, the current study's reflection of the convective heating effect, which controls the temperature of the stretched surface, may have contributed to this phenomenon. In reality, increased convection causes higher surface temperatures, allowing the thermal impact to go deeper into the nanofluid. Next, Figure 4 illustrates the magnetic parameter  $M$  effect on the temperature profile  $\theta(\eta)$ . Having higher levels of the magnetic parameter  $M$ , the temperature  $\theta(\eta)$  becomes greater for all types of nanoparticle shapes. The Lorentz force, which acts as a reverse force when magnetic effect is present, causes this. This force increases the fluid's friction by opposing the fluid's motion. It is a resistive force; hence, fluid friction causes the temperature to rise. Figure 5 illustrates the effect with respect to the mixed convection parameter  $\lambda$  towards the temperature profile  $\theta(\eta)$ . Furthermore, note that the temperature  $\theta(\eta)$  reduces provided the buoyancy parameter boosts (from opposing to assisting). However, it is important to point out that, for platelet and cylinder shapes, the temperature receives less impact. Near the wall, the assisting flow has a lower temperature than the opposing flow. The assisting flow, in theory, transfers heat from the hot plate to the cool fluid, eventually bringing the wall temperature down.



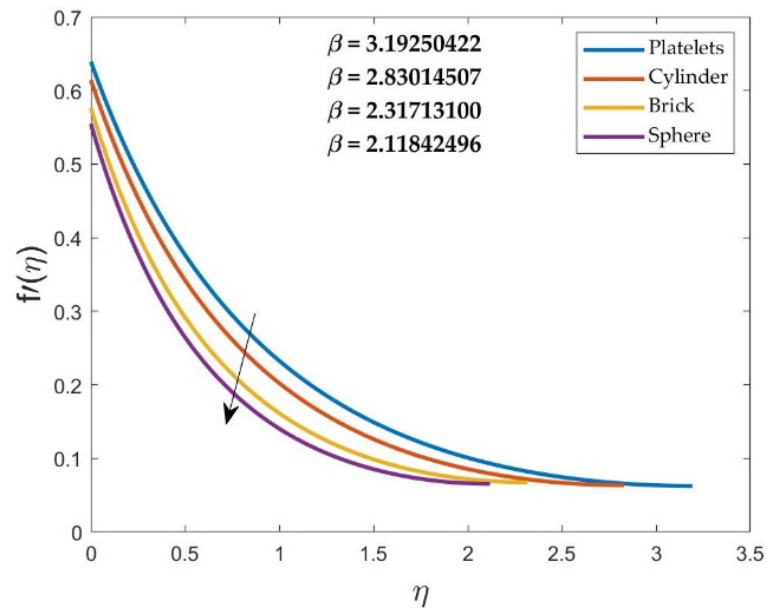


Figure 2. Impact of shape factor on velocity profile for  $S = 0.4$ ,  $M = 1.0$ ,  $K = 0.5$  and  $\varphi = 0.02$ .

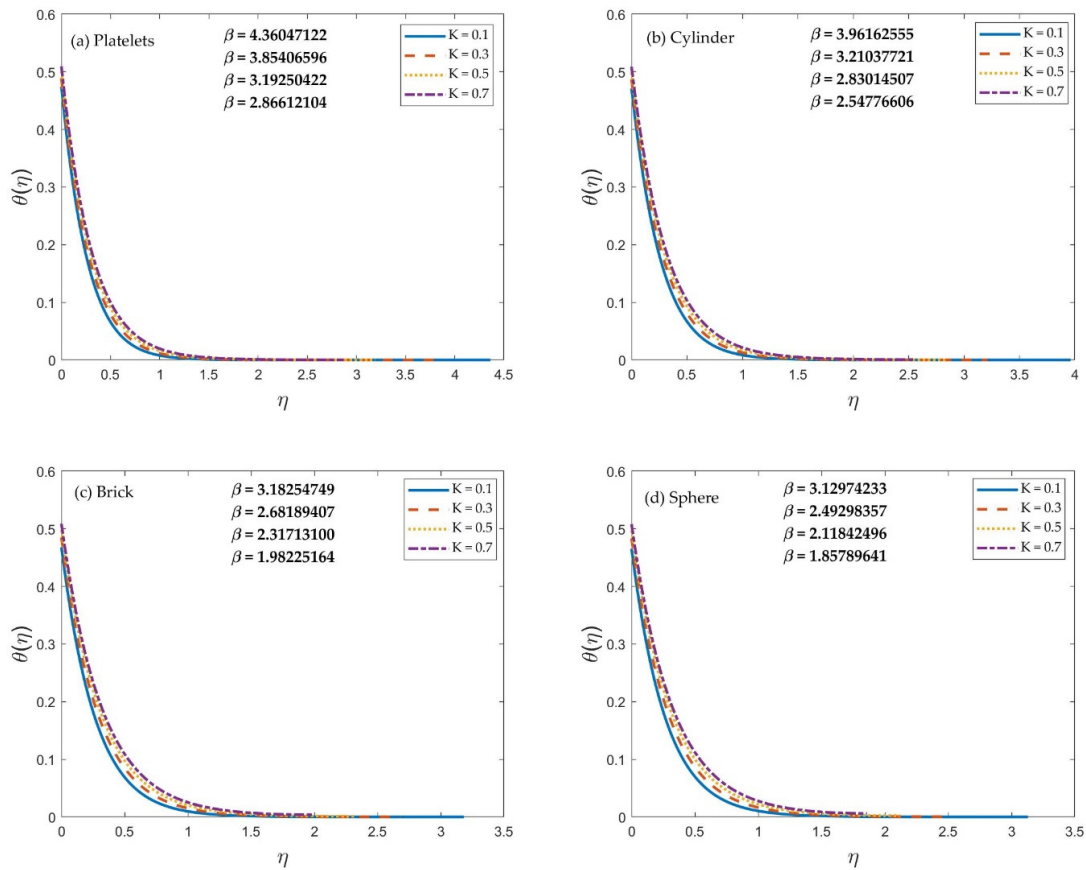
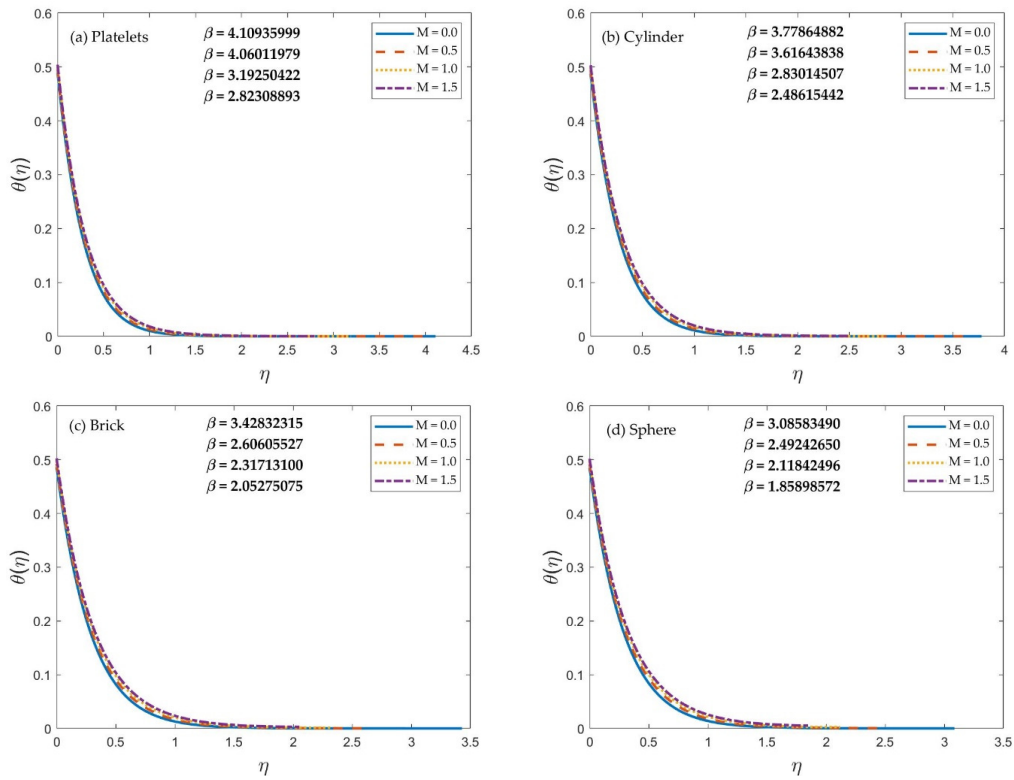
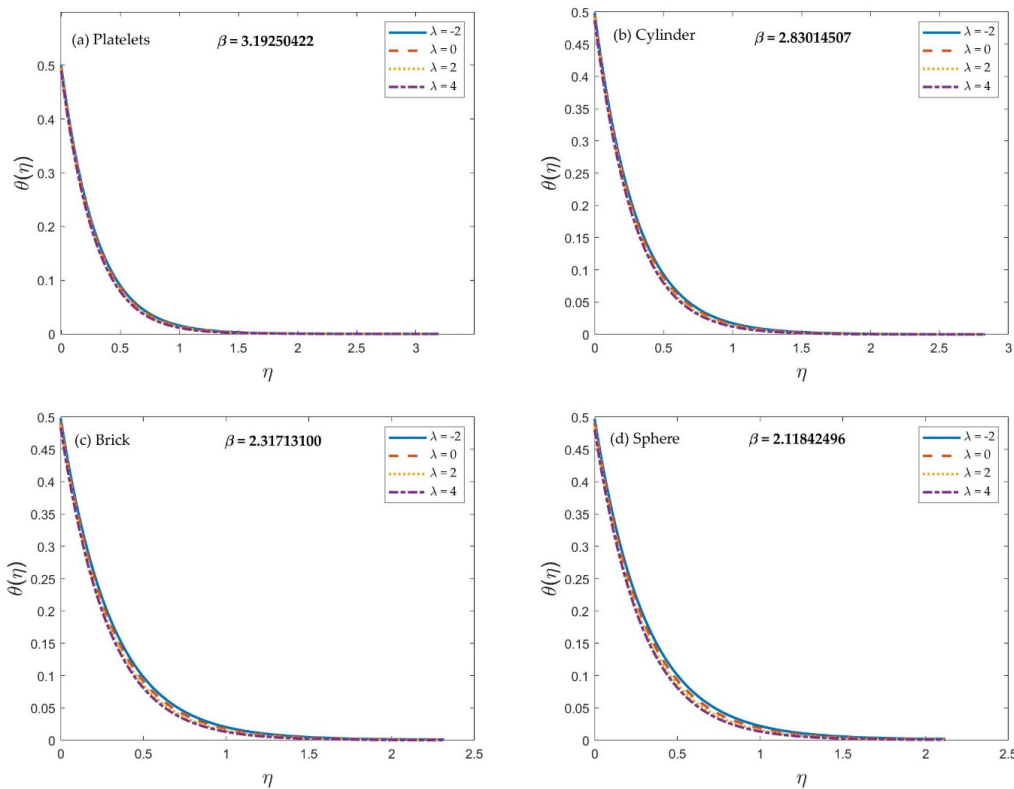


Figure 3. Impact of the slip parameter  $K$  on the temperature profile for  $S = 0.4$ ,  $\varphi = 0.02$ ,  $M = 1.0$ ,  $Bi = 3.0$ ,  $\lambda = -2.0$ ,  $\alpha = \pi/4$  and  $Pr = 8.0$ .



**Figure 4.** Impact of the magnetic parameter  $M$  on the temperature profile for  $S = 0.4$ ,  $K = 0.5$ ,  $\varphi = 0.02$ ,  $Bi = 3.0$ ,  $\lambda = -2.0$ ,  $\alpha = \pi/4$  and  $Pr = 8.0$ .



**Figure 5.** Impact of the mixed convection parameter  $\lambda$  on the temperature profile for  $S = 0.4$ ,  $K = 0.5$ ,  $\varphi = 0.02$ ,  $M = 1.0$ ,  $Bi = 3.0$ ,  $\alpha = \pi/4$  and  $Pr = 8.0$ .

The temperature profile  $\theta(\eta)$  behavior for different inclination angle parameters  $\alpha$  values are shown in Figure 6. It is discovered that, as the angle of inclination parameter  $\alpha$  increases, the temperature  $\theta(\eta)$  for all multi-shape nanosize particles decreases. The buoyancy force increases when the inclination to the horizontal increases. Physically, when the sheet is oriented vertically, the strongest gravitational forces have an impact on the flow. However, if the plate is turned from vertical to horizontal (and as the value of  $\alpha$  increases), the buoyancy force increases. Thus, the thermal boundary layer reduces. It is noticed that the problem is reduced to the vertical plate if  $\alpha = 0^\circ$ , whereas when  $\alpha = 90^\circ$  the problem is lowered to the horizontal plate. It is noted that for  $\alpha = 30^\circ, 45^\circ, 60^\circ$ , the problem reduces to the inclined plate. Figure 7 shows the Biot number  $Bi$  effect on the temperature profile  $\theta(\eta)$ . Moreover, it is discovered that raising  $Bi$  increases the fluid temperature. Additionally,  $Bi$  is calculated by dividing convection at the surface by conduction inside the body surface. Convection will become more potent near the surface as a consequence of the increase in  $Bi$ , leading to an increase in the thickness of the thermal boundary layer. Additionally, as illustrated in Figure 8, the temperature rises as the film's thickness reduces as the shape of the nanoparticles shifts from platelet to spherical. It should be noted that the shape factor has a greater impact on platelet shape than other factors. In Figure 9, the magnetic parameter  $M$  and unsteadiness parameter  $S$  impacts on the film thickness  $\beta$  are depicted. The decreasing trends in film thickness  $\beta$  are shown in this figure for every multi-shape nanoparticle when the unsteadiness parameter  $S$  increases, coupled with a rise in the magnetic parameter  $M$ . Also, when  $S \rightarrow 0$ , as shown in Figure 9, it represents the liquid film thickness of an infinite thickness ( $\beta \rightarrow \infty$ ). For the particular values  $S_0$  of  $S$ , no solutions can be obtained, while  $S \rightarrow S_0$  represents the case of an infinitesimal thick fluid layer ( $\beta \rightarrow 0$ ).

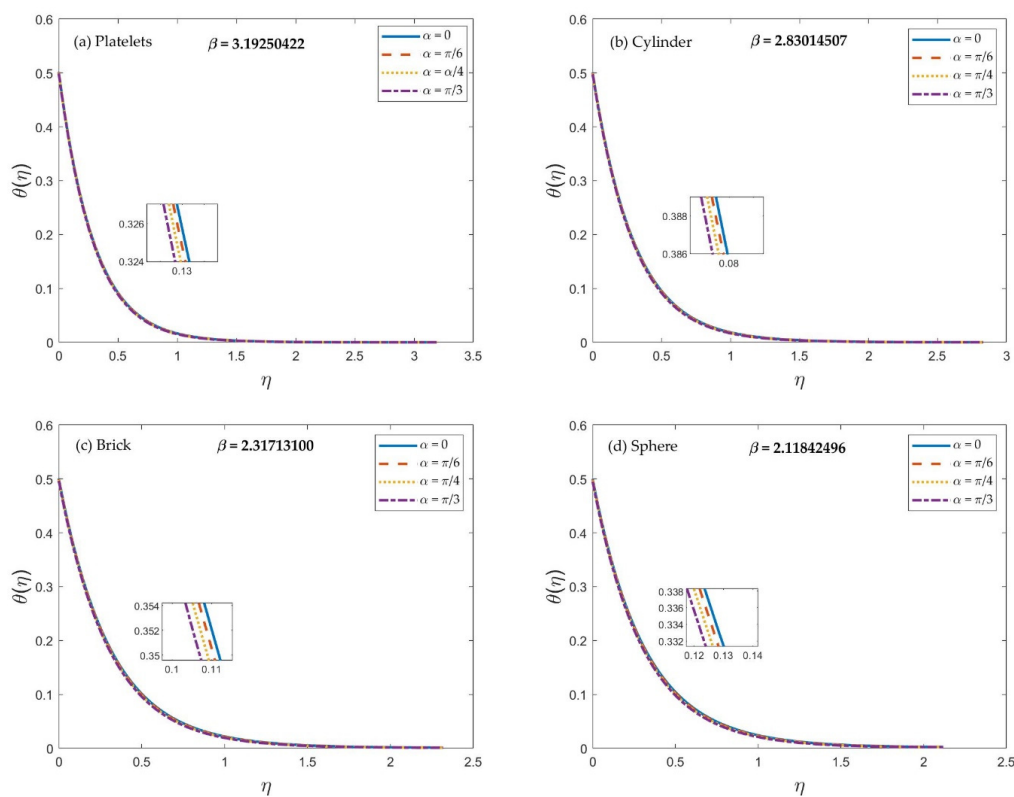


**Figure 6.** Impact of the inclination angle parameters  $\alpha$  on the temperature profile for  $S = 0.4, K = 0.5, \varphi = 0.02, M = 1.0, Bi = 3.0, \lambda = -2.0$  and  $Pr = 8.0$ .

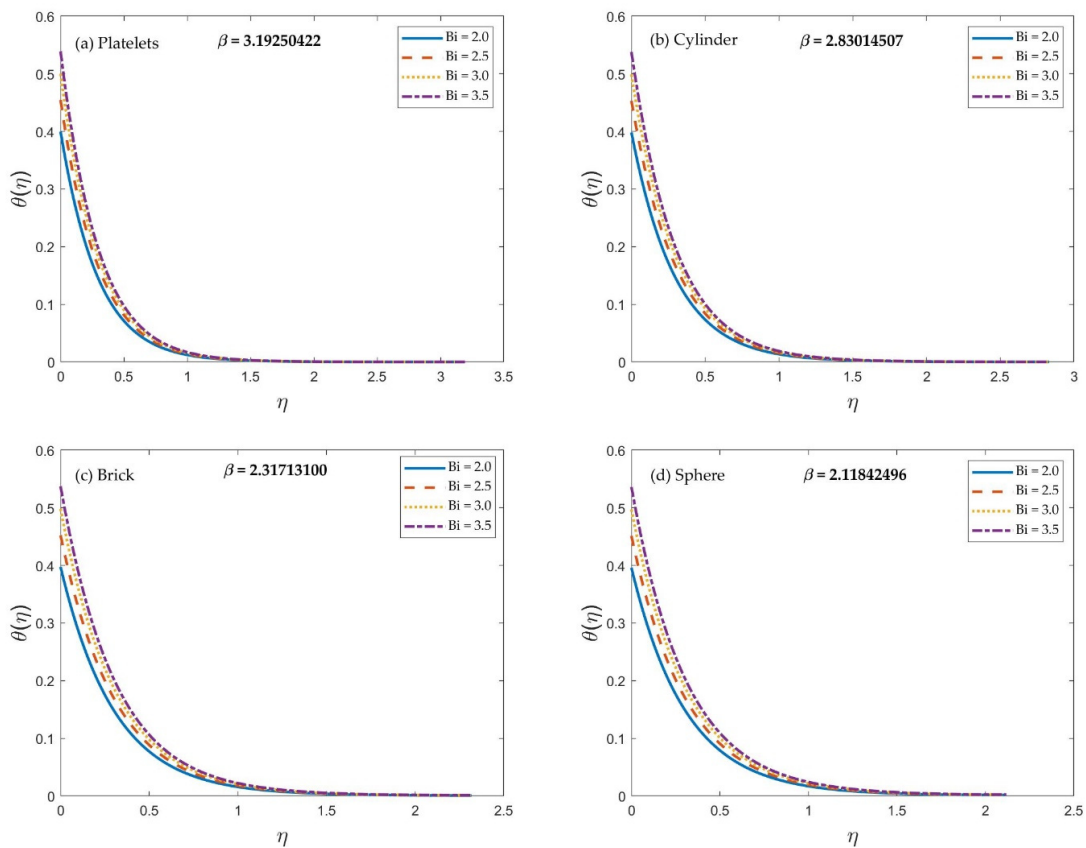


**Figure 7.** Impact of the Biot number  $Bi$  on the temperature profile for  $S = 0.4, K = 0.5, \varphi = 0.02, M = 1.0, \lambda = -2.0, \alpha = \pi/4$  and  $Pr = 8.0$ .

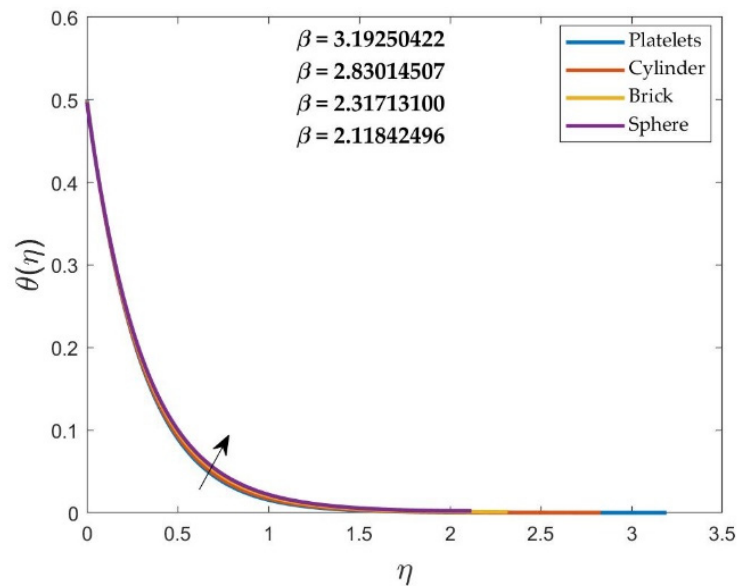


**Figure 8.** Impact of shape factor on the temperature profile for  $S = 0.4, K = 0.5, \varphi = 0.02, M = 1.0, Bi = 3.0, \lambda = -2.0, \alpha = \pi/4$  and  $Pr = 8.0$ .

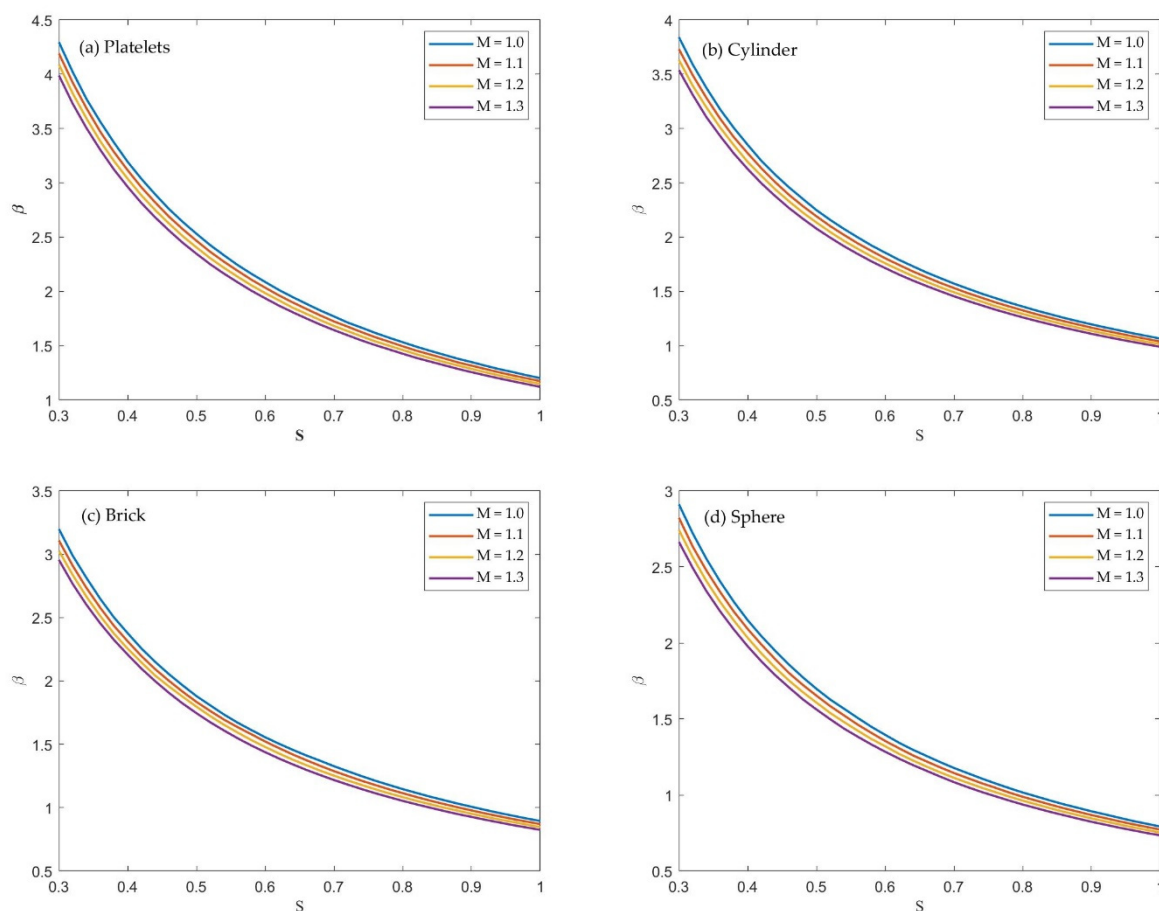


**Figure 9.** The film thickness  $\beta$  against the unsteadiness parameter  $S$  for diverse values of  $M$  when  $K = 0.5$  and  $\varphi = 0.02$ .

## 5. Conclusions

A numerical study has been done on the unsteady thin film flow and the heat transfer of  $\text{Al}_2\text{O}_3/\text{water}$  nanofluid steered by an inclined stretching sheet. Applying similarity transformation, the governing partial differential equations (PDEs) are reduced to a set of ordinary differential equations (ODEs), which are then numerically solved via the boundary value problem solver (bvp4c) in the Matlab software. The findings are listed below:

- Provided that the magnetic parameter  $M$  and the slip parameter  $K$  rise, the film thickness  $\beta$  reduces.
- The temperature  $\theta(\eta)$  enhances as the Biot number  $Bi$  boosts. For platelet-shaped particles, the film thickness is high, whereas, for cylinder, brick, and sphere-shaped nanoparticles, it ultimately diminishes.
- On the platelet and sphere shape nanoparticles, the velocity of  $\text{Al}_2\text{O}_3$  nanofluid achieves its maximum and minimum, whereas a different pattern can be seen in the temperature.
- The skin friction coefficient lessens when the slip and mixed convection parameters rise. In contrast, incrementally the volume fraction and magnetic parameters increase the skin friction coefficient.
- The local Nusselt number increases as the Biot number  $Bi$ , inclination angle, and mixed convection parameters increase, while it declines with an augmentation in the slip and magnetic parameters.
- The assisting buoyancy flow ( $\lambda > 0$ ) appears to have a greater local Nusselt number than the opposing buoyancy flow ( $\lambda < 0$ ), despite the fact that the skin friction coefficient produces the opposite outcome.

- A decrease in film thickness is produced by a rise in the unsteadiness parameter, as well as the magnetic parameter.

**Author Contributions:** Conceptualization, A.I. and S.E.A.; funding acquisition, A.I.; methodology, S.A. and I.W.; Project administration, A.I.; supervision, A.I., S.A.B. and S.E.A.; validation, I.W., S.A.B., A.I. and S.E.A.; writing—original draft, S.A.; writing—review and editing, A.I., S.A.B., I.W. and S.E.A. All authors have read and agreed to the published version of the manuscript.

**Funding:** This research was funded by Universiti Kebangsaan Malaysia (Project Code: DIP-2020-001).

**Data Availability Statement:** Not applicable.

**Conflicts of Interest:** The authors declare no conflict of interest.

## Nomenclature

$a : b$	dimensional constants ( $s^{-1}$ )
$Bi$	Biot number
$B_0$	uniform magnetic field
$c_p$	specific heat of the fluid ( $J\ kg^{-1}K^{-1}$ )
$g$	acceleration due to gravity ( $m\ s^{-2}$ )
$Gr$	Grashof number
$h(t)$	film thickness (m)
$k$	thermal conductivity of the fluid ( $W\ m^{-1}K^{-1}$ )
$M$	magnetic parameter
$Nu$	Nusselt number
$Pr$	Prandtl number
$Re$	Reynolds number
$S$	unsteadiness parameter
$t$	time (s)
$T$	fluid temperature (K)
$T_w$	surface temperature at the wall (K)
$T_0$	reference temperature (K)
$T_\infty$	ambient temperature (K)
$U_w$	surface velocity ( $m\ s^{-1}$ )
$u, v$	velocity components in the $x$ and $y$ directions ( $m\ s^{-1}$ )
$x, y$	Cartesian coordinates (m)
Greek symbols	
$\alpha$	inclination angle
$\beta$	dimensionless film thickness
$\beta^*$	thermal expansion coefficient of the fluid ( $K^{-1}$ )
$\eta$	similarity variable
$\lambda$	mixed convection parameter
$\mu$	dynamic viscosity of the fluid ( $kg\ m^{-1}s^{-1}$ )
$\nu$	kinematic viscosity of the fluid ( $m^2\ s^{-1}$ )
$\varphi$	dimensionless nanoparticle volume fraction
$\psi$	stream function ( $m^2\ s^{-1}$ )
$\rho$	density of the fluid ( $kg\ m^{-3}$ )
$(\rho c_p)$	heat capacity of the fluid ( $J\ K^{-1}m^{-3}$ )
$\sigma$	electrical conductivity of the fluid ( $s\ m^{-1}$ )
$\theta$	dimensionless temperature
Subscripts	
$f$	base fluid
$nf$	Nanofluid
$s$	solid nanoparticle
$w$	condition at the wall
Superscript	
'	differentiation with respect to $\eta$

## References

1. Waini, I.; Ishak, A.; Pop, I. Unsteady flow and heat transfer past a stretching/shrinking sheet in a hybrid nanofluid. *Int. J. Heat Mass Transf.* **2019**, *136*, 288–297. [\[CrossRef\]](#)
2. Choi, S.U.S.; Eastman, J.A. *Enhancing Thermal Conductivity of Fluids with Nanoparticles*; Argonne National Lab.: Lemont, IL, USA, 1995.
3. Choi, S.U.S. Nanofluids: From vision to reality through research. *J. Heat Transfer.* **2009**, *131*, 033106. [\[CrossRef\]](#)
4. Senthilraja, S.; Karthikeyan, M.; Gangadevi, R. Nanofluid applications in future automobiles: Comprehensive review of existing data. *Nano-Micro Lett.* **2010**, *2*, 306–310. [\[CrossRef\]](#)
5. Saidur, R.; Leong, K.Y.; Mohammed, H.A. A review on applications and challenges of nanofluids. *Renew. Sustain. Energy Rev.* **2011**, *15*, 1646–1668. [\[CrossRef\]](#)
6. Sheremet, M.A. Applications of nanofluids. *Nanomaterials* **2021**, *11*, 1716. [\[CrossRef\]](#)
7. Waini, I.; Ishak, A.; Pop, I. Nanofluid flow on a shrinking cylinder with  $\text{Al}_2\text{O}_3$  nanoparticles. *Mathematics* **2021**, *9*, 1612. [\[CrossRef\]](#)
8. Hamid, K.A.; Azmi, W.H.; Mamat, R.; Sharma, K. V Heat transfer performance of  $\text{TiO}_2$ – $\text{SiO}_2$  nanofluids in a tube with wire coil inserts. *Appl. Therm. Eng.* **2019**, *152*, 275–286. [\[CrossRef\]](#)
9. Safwa Khashi'ie, N.; Md Arifin, N.; Hafidzuddin, E.H.; Wahi, N. Dual stratified nanofluid flow past a permeable shrinking/stretching sheet using a non-Fourier energy model. *Appl. Sci.* **2019**, *9*, 2124. [\[CrossRef\]](#)
10. Anwar, M.I.; Rafique, K.; Misiran, M.; Khan, I. Numerical solution of casson nanofluid flow over a non-linear inclined surface with solet and dufour effects by keller-box method. *Front. Phys.* **2019**, *7*, 139.
11. Bachok, N.; Ishak, A.; Pop, I. Boundary-layer flow of nanofluids over a moving surface in a flowing fluid. *Int. J. Therm. Sci.* **2010**, *49*, 1663–1668. [\[CrossRef\]](#)
12. Zaimi, K.; Ishak, A.; Pop, I. Flow past a permeable stretching/shrinking sheet in a nanofluid using two-phase model. *PLoS ONE* **2014**, *9*, e111743. [\[CrossRef\]](#)
13. Salleh, S.N.A.; Bachok, N.; Arifin, N.M.; Ali, F.M. Numerical analysis of boundary layer flow adjacent to a thin needle in nanofluid with the presence of heat source and chemical reaction. *Symmetry* **2019**, *11*, 543. [\[CrossRef\]](#)
14. Sajjadi, H.; Delouei, A.A.; Atashafrooz, M.; Sheikholeslami, M. Double MRT Lattice Boltzmann simulation of 3-D MHD natural convection in a cubic cavity with sinusoidal temperature distribution utilizing nanofluid. *Int. J. Heat Mass Transf.* **2018**, *126*, 489–503. [\[CrossRef\]](#)
15. Atashafrooz, M.; Sajjadi, H.; Amiri Delouei, A.; Yang, T.-F.; Yan, W.-M. Three-dimensional analysis of entropy generation for forced convection over an inclined step with presence of solid nanoparticles and magnetic force. *Numer. Heat Transf. Part A Appl.* **2021**, *80*, 318–335. [\[CrossRef\]](#)
16. Crane, L.J. Flow past a stretching plate. *Zeitschrift für Angew. Math. und Phys.* **1970**, *21*, 645–647. [\[CrossRef\]](#)
17. Gupta, P.S.; Gupta, A.S. Heat and mass transfer on a stretching sheet with suction or blowing. *Can. J. Chem. Eng.* **1977**, *55*, 744–746. [\[CrossRef\]](#)
18. Sharma, R.; Ishak, A.; Pop, I. Partial slip flow and heat transfer over a stretching sheet in a nanofluid. *Math. Probl. Eng.* **2013**, *2013*, 724547. [\[CrossRef\]](#)
19. Zokri, S.M.; Arifin, N.S.; Salleh, M.Z.; Kasim, A.R.M.; Mohammad, N.F.; Yusoff, W. MHD Jeffrey nanofluid past a stretching sheet with viscous dissipation effect. *J. Phys. Conf. Ser.* **2017**, *890*, 12002. [\[CrossRef\]](#)
20. Kho, Y.B.; Hussanan, A.; Mohamed, M.K.A.; Sarif, N.M.; Ismail, Z.; Salleh, M.Z. Thermal radiation effect on MHD Flow and heat transfer analysis of Williamson nanofluid past over a stretching sheet with constant wall temperature. *J. Phys. Conf. Ser.* **2017**, *890*, 12034. [\[CrossRef\]](#)
21. Daniel, Y.S.; Aziz, Z.A.; Ismail, Z.; Salah, F. Thermal stratification effects on MHD radiative flow of nanofluid over nonlinear stretching sheet with variable thickness. *J. Comput. Des. Eng.* **2018**, *5*, 232–242. [\[CrossRef\]](#)
22. Ahmed, S.E.; Mohamed, R.A.; Abd Elraheem, M.A.; Soliman, M.S. Magnetohydrodynamic Maxwell nanofluids flow over a stretching surface through a porous medium: Effects of non-linear thermal radiation, convective boundary conditions and heat generation/absorption. *World Acad. Sci. Eng.* **2019**, *13*, 436–443.
23. Kho, Y.B.; Hussanan, A.; Sarif, N.M.; Ismail, Z.; Salleh, M.Z. Thermal radiation effects on MHD with flow heat and mass transfer in Casson nanofluid over a stretching sheet. In Proceedings of the MATEC Web of Conferences, Penang, Malaysia, 6–7 December 2017; EDP Sciences: Ulis, France, 2018; Volume 150, p. 6036.
24. Ibrahim, W.; Negera, M. MHD slip flow of upper-convected Maxwell nanofluid over a stretching sheet with chemical reaction. *J. Egypt. Math. Soc.* **2020**, *28*, 7. [\[CrossRef\]](#)
25. Prasannakumara, B.C. Numerical simulation of heat transport in Maxwell nanofluid flow over a stretching sheet considering magnetic dipole effect. *Partial Differ. Equ. Appl. Math.* **2021**, *4*, 100064. [\[CrossRef\]](#)
26. Hazarika, S.; Ahmed, S.; Chamkha, A.J. Investigation of nanoparticles Cu, Ag and  $\text{Fe}_3\text{O}_4$  on thermophoresis and viscous dissipation of MHD nanofluid over a stretching sheet in a porous regime: A numerical modeling. *Math. Comput. Simul.* **2021**, *182*, 819–837. [\[CrossRef\]](#)
27. Gupta, S.; Kumar, D.; Singh, J. MHD mixed convective stagnation point flow and heat transfer of an incompressible nanofluid over an inclined stretching sheet with chemical reaction and radiation. *Int. J. Heat Mass Transf.* **2018**, *118*, 378–387. [\[CrossRef\]](#)
28. Usman, M.; Soomro, F.A.; Haq, R.U.; Wang, W.; Deftlerli, O. Thermal and velocity slip effects on Casson nanofluid flow over an inclined permeable stretching cylinder via collocation method. *Int. J. Heat Mass Transf.* **2018**, *122*, 1255–1263. [\[CrossRef\]](#)

29. Kumar, B.; Srinivas, S. Unsteady hydromagnetic flow of Eyring-Powell nanofluid over an inclined permeable stretching sheet with joule heating and thermal radiation. *J. Appl. Comput. Mech.* **2020**, *6*, 259–270.
30. Soomro, F.A.; Usman, M.; El-Sapa, S.; Hamid, M.; Haq, R.U. Numerical study of heat transfer performance of MHD  $\text{Al}_2\text{O}_3$ -Cu/water hybrid nanofluid flow over inclined surface. *Arch. Appl. Mech.* **2022**, *92*, 2757–2765. [[CrossRef](#)]
31. Schlichting, H.; Gersten, K. *Boundary-Layer Theory*; Springer Science & Business Media: Berlin/Heidelberg, Germany, 2003; ISBN 3540662707.
32. Smith, F.T. Steady and unsteady boundary-layer separation. *Annu. Rev. Fluid Mech.* **1986**, *18*, 197–220. [[CrossRef](#)]
33. White, F.M.; Majdalani, J. *Viscous Fluid Flow*; McGraw-Hill: New York, NY, USA, 2006.
34. Ishak, A.; Nazar, R.; Pop, I. Boundary layer flow and heat transfer over an unsteady stretching vertical surface. *Meccanica* **2009**, *44*, 369–375. [[CrossRef](#)]
35. Ishak, A. Unsteady MHD flow and heat transfer over a stretching plate. *J. Appl. Sci.* **2010**, *10*, 2127–2131. [[CrossRef](#)]
36. Daniel, Y.S.; Aziz, Z.A.; Ismail, Z.; Salah, F. Slip effects on electrical unsteady MHD natural convection flow of nanofluid over a permeable shrinking sheet with thermal radiation. *Eng. Lett.* **2018**, *26*, 1–13.
37. Dzulkipli, N.F.; Bachok, N.; Yacob, N.A.; Md Arifin, N.; Rosali, H. Unsteady stagnation-point flow and heat transfer over a permeable exponential stretching/shrinking sheet in nanofluid with slip velocity effect: A stability analysis. *Appl. Sci.* **2018**, *8*, 2172. [[CrossRef](#)]
38. Waini, I.; Ishak, A.; Pop, I. Unsteady hybrid nanofluid flow on a stagnation point of a permeable rigid surface. *ZAMM-J. Appl. Math. Mech. für Angew. Math. und Mech.* **2021**, *101*, e202000193. [[CrossRef](#)]
39. Zainal, N.A.; Nazar, R.; Naganthran, K.; Pop, I. Stability Analysis of Unsteady Hybrid Nanofluid Flow Past a Permeable Stretching/Shrinking Cylinder. *J. Adv. Res. Fluid Mech. Therm. Sci.* **2021**, *86*, 64–75. [[CrossRef](#)]
40. Wang, C.Y. Liquid film on an unsteady stretching surface. *Q. Appl. Math.* **1990**, *48*, 601–610. [[CrossRef](#)]
41. Andersson, H.I.; Aarseth, J.B.; Dandapat, B.S. Heat transfer in a liquid film on an unsteady stretching surface. *Int. J. Heat Mass Transf.* **2000**, *43*, 69–74. [[CrossRef](#)]
42. Khan, N.S.; Islam, S.; Gul, T.; Khan, I.; Khan, W.; Ali, L. Thin film flow of a second grade fluid in a porous medium past a stretching sheet with heat transfer. *Alexandria Eng. J.* **2018**, *57*, 1019–1031. [[CrossRef](#)]
43. Naganthran, K.; Hashim, I.; Nazar, R. Triple Solutions of Carreau Thin Film Flow with Thermocapillarity and Injection on an Unsteady Stretching Sheet. *Energies* **2020**, *13*, 3177. [[CrossRef](#)]
44. Naganthran, K.; Nazar, R.; Siri, Z.; Hashim, I. Entropy Analysis and Melting Heat Transfer in the Carreau Thin Hybrid Nanofluid Film Flow. *Mathematics* **2021**, *9*, 3092. [[CrossRef](#)]
45. Ali, R.; Shahzad, A.; us Saher, K.; Elahi, Z.; Abbas, T. The thin film flow of  $\text{Al}_2\text{O}_3$  nanofluid particle over an unsteady stretching surface. *Case Stud. Therm. Eng.* **2022**, *29*, 101695. [[CrossRef](#)]
46. Tiwari, R.K.; Das, M.K. Heat transfer augmentation in a two-sided lid-driven differentially heated square cavity utilizing nanofluids. *Int. J. Heat Mass Transf.* **2007**, *50*, 2002–2018. [[CrossRef](#)]
47. Alabdulhadi, S.; Waini, I.; Ahmed, S.E.; Ishak, A. Hybrid Nanofluid Flow and Heat Transfer Past an Inclined Surface. *Mathematics* **2021**, *9*, 3176. [[CrossRef](#)]
48. Nasir, S.; Shah, Z.; Islam, S.; Bonyah, E.; Gul, T. Darcy Forchheimer nanofluid thin film flow of SWCNTs and heat transfer analysis over an unsteady stretching sheet. *AIP Adv.* **2019**, *9*, 15223. [[CrossRef](#)]
49. Vajjha, R.S.; Das, D.K. Experimental determination of thermal conductivity of three nanofluids and development of new correlations. *Int. J. Heat Mass Transf.* **2009**, *52*, 4675–4682. [[CrossRef](#)]
50. Oztop, H.F.; Abu-Nada, E. Numerical study of natural convection in partially heated rectangular enclosures filled with nanofluids. *Int. J. Heat Fluid Flow* **2008**, *29*, 1326–1336. [[CrossRef](#)]
51. Timofeeva, E.V.; Routbort, J.L.; Singh, D. Particle shape effects on thermophysical properties of alumina nanofluids. *J. Appl. Phys.* **2009**, *106*, 14304. [[CrossRef](#)]
52. Schlichting, H.; Gersten, K. *Boundary Layer Theory*; Springer: Berlin/Heidelberg, Germany, 2017.
53. Shampine, L.F.; Gladwell, I.; Thompson, S. *Solving ODEs with MATLAB*; Cambridge University Press: Cambridge, UK, 2003; ISBN 9780521824040.
54. Abel, M.S.; Mahesha, N.; Tawade, J. Heat transfer in a liquid film over an unsteady stretching surface with viscous dissipation in presence of external magnetic field. *Appl. Math. Model.* **2009**, *33*, 3430–3441. [[CrossRef](#)]

**Disclaimer/Publisher's Note:** The statements, opinions and data contained in all publications are solely those of the individual author(s) and contributor(s) and not of MDPI and/or the editor(s). MDPI and/or the editor(s) disclaim responsibility for any injury to people or property resulting from any ideas, methods, instructions or products referred to in the content.